

LETTER TO THE EDITOR

The Extreme Ultraviolet and X-Ray Sun in Time: High-Energy Evolutionary Tracks of a Solar-Like Star

Lin Tu¹, Colin P. Johnstone¹, Manuel Güdel¹, and Helmut Lammer²

¹Department of Astrophysics, University of Vienna, Türkenschanzstrasse 17, A-1180 Vienna
e-mail: lin.tu@univie.ac.at, colin.johnstone@univie.ac.at, manuel.guedel@univie.ac.at
²Space Research Institute, Austrian Academy of Sciences, Schmiedlstrasse 6, A-8042 Graz, Austria
e-mail: helmut.lammer@oeaw.ac.at

Received August 10, 2014; accepted ...

ABSTRACT

Aims. We aim to describe the pre-main sequence and main-sequence evolution of X-ray and extreme-ultraviolet radiation of a solar mass star based on its rotational evolution starting with a realistic range of initial rotation rates.

Methods. We derive evolutionary tracks of X-ray radiation based on a rotational evolution model for solar mass stars and the rotation-activity relation. We compare these tracks to X-ray luminosity distributions of stars in clusters with different ages.

Results. We find agreement between the evolutionary tracks derived from rotation and the X-ray luminosity distributions from observations. Depending on the initial rotation rate, a star might remain at the X-ray saturation level for very different time periods, from ≈ 10 Myr to ≈ 300 Myr for slow and fast rotators, respectively.

Conclusions. Rotational evolution with a spread of initial conditions leads to a particularly wide distribution of possible X-ray luminosities in the age range of 20–500 Myrs, before rotational convergence and therefore X-ray luminosity convergence sets in. This age range is crucial for the evolution of young planetary atmospheres and may thus lead to very different planetary evolution histories.

Key words. stars: pre-main sequence – X-rays: stars

1. Introduction

High-energy radiation from solar-like main-sequence (MS) stars decays in time owing to stellar spin-down. The early Sun's X-ray ($\approx 1 - 100$ Å) and extreme-ultraviolet ($\approx 100 - 900$ Å) emissions could thus have exceeded the present-day Sun's level by orders of magnitude (Ribas et al. 2005). By driving atmospheric erosion, such extreme radiation levels were critically important for both the primordial hydrogen atmospheres (e.g., Lammer et al. 2014) and the secondary nitrogen atmospheres (Lichtenegger et al. 2010) of solar system planets. As a consequence of higher solar activity levels, stronger winds would have added to atmospheric mass loss through non-thermal processes such as ion pick-up (Kislyakova et al. 2013; Kislyakova et al. 2014).

Magnetic activity is strongly coupled to rotation via a stellar dynamo, such that the total X-ray luminosity decays with increasing rotation period, P , as $L_X \propto P^{-3}$ to $\propto P^{-2}$; for small P , L_X saturates at $L_X \approx 10^{-3} L_{\text{bol}}$ (L_{bol} being the stellar bolometric luminosity; see Wright et al. 2011=W11). Since older (>1 Gyr) stars spin down in time approximately as $P \propto t^{0.5}$ (Skumanich 1972), L_X decays as $L_X \propto t^{-1.5}$ (Güdel et al. 1997). This evolutionary trend has commonly been formulated using regression fits to L_X of stars with known ages, typically starting at the saturation level close to the zero-age main-sequence (ZAMS; see, e.g., Güdel et al. 1997; Ribas et al. 2005).

However, stars in young stellar clusters have a wide spread in rotation rates, Ω , in particular at ages younger than 500 Myr before they converge to a unique mass-dependent value (Soderblom et al. 1993). As a consequence, L_X values also scat-

ter over a wide range among such stars (e.g., Stauffer et al. 1994), and the age at which stars fall out of saturation depends on the star's initial Ω . Given the importance of high-energy radiation in this age range for planetary atmosphere evolution, a unique description with a single radiation decay law is problematic and needs to be replaced by a description of the L_X distribution and its long-term evolution (Penz et al. 2008; Johnstone et al. 2015), spanning a wide range of possible evolutionary tracks for stars with different initial Ω .

In this Letter, we use a rotational evolution model to predict such luminosity distributions as a function of age, based on a range of initial Ω , and we show that these predictions agree with the observed time-dependent scatter of L_X . We derive a radiative evolution model based on the full range of rotation histories for a solar-mass star, and thus find a description of the possible past histories of our own Sun, which is useful to model the corresponding evolution of solar-system planetary atmospheres. This Letter is an extension of Johnstone et al. (2015), who similarly estimated evolutionary tracks for wind properties. In this Letter, we concentrate mostly on $1 M_{\odot}$ stars, and will extend this to other stellar masses in future work.

2. Rotation and Radiation Models

As in previous studies (e.g. Gallet & Bouvier 2013), we constrain our rotation models by assuming that the percentiles of the rotational distributions for star clusters with different ages can be combined to estimate the time evolution of a star's rotation rate. We consider only stars in the mass range $0.9 M_{\odot}$ to $1.1 M_{\odot}$. Johnstone et al. (2015) collected measured rotation pe-

arXiv:1504.04546v1 [astro-ph.SR] 17 Apr 2015

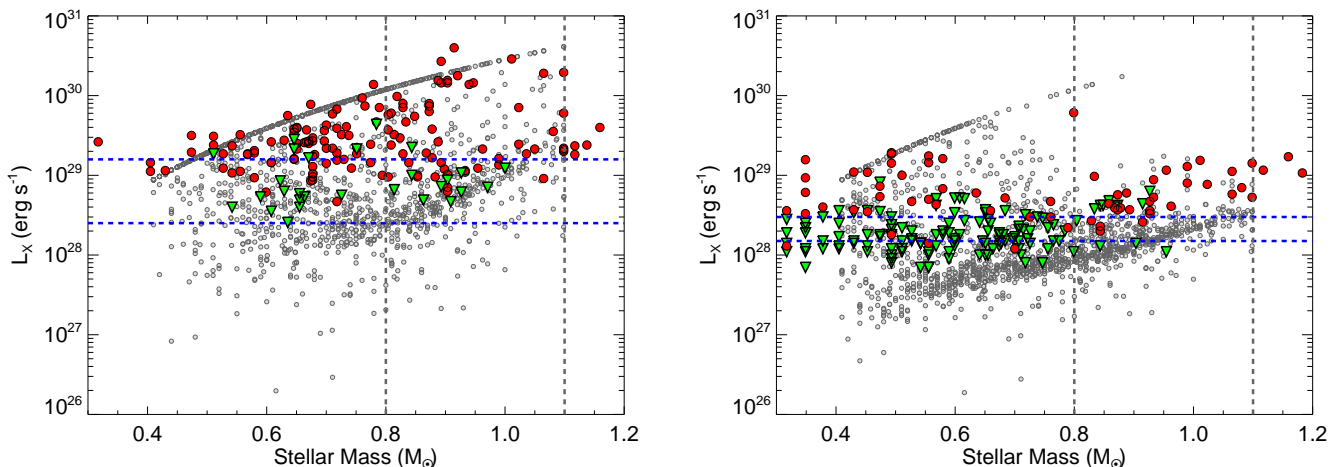


Fig. 1. Comparisons between observed and predicted distributions of L_X at ages of 150 Myr (*left*) and 620 Myr (*right*). The grey symbols show predicted distributions calculated using Eqn. 1 and the distributions of rotation rates derived by Johnstone et al. (2015). The red circles and green triangles show detections and upper limits for stars in the Pleiades (*left*) and Hyades (*right*). The horizontal blue lines show detection thresholds. The upper line of stars in the theoretical distributions is caused by the stars whose rotation rates lie above the mass dependent saturation threshold.

riods of over 2000 stars in clusters of ages 150, 550, and 1000 Myr on the MS, giving observational constraints on the percentiles at these ages (with 230, 134, and 36 stars, respectively at the considered ages). We use additional constraints for pre-main sequence (PMS) rotation from the ≈ 2 Myr cluster NGC 6530 (28 stars; Henderson & Stassun 2012) and the ≈ 12 Myr cluster h Per (117 stars; Moraux et al. 2013). For NGC 6530, the 10th, 50th, and 90th percentiles are at $2.7\Omega_\odot$, $6.2\Omega_\odot$, and $35.1\Omega_\odot$, respectively (assuming $\Omega_\odot = 2.9 \times 10^{-6}$ rad s^{-1}), and for h Per, they are at $3.4\Omega_\odot$, $8.4\Omega_\odot$, and $76.0\Omega_\odot$, respectively.

We use an extension of the rotational evolution model of Johnstone et al. (2015). For the wind torque, we use the formula derived by Matt et al. (2012) which relates the wind torque to stellar parameters, the star’s dipole field strength, B_{dip} , and the wind mass loss rate, \dot{M}_* . We assume that both B_{dip} and \dot{M}_* saturate at a Rossby number of $Ro = 0.13$, as suggested by the saturation of X-ray emission (W11), where $Ro = P_{\text{rot}}/\tau_*$ and τ_* is the convective turnover time. For \dot{M}_* , we use the scaling law derived by Johnstone et al. (2015), which is derived by fitting the rotational evolution model to observational constraints. We modify the scaling law by relating \dot{M}_* to Ro ; this allows us to take into account the change in τ_* on the PMS. Since we only consider solar mass stars, the scaling relation derived by Johnstone et al. (2015) can be rewritten as $\dot{M}_* \propto R_*^2 Ro^{-a}$. We find $a = 2$ provides a good fit to the observational constraints (which is larger than the value of $a = 1.33$ found by Johnstone et al. 2015). For B_{dip} , we use the scaling law derived by Vidotto et al. (2014) of $B_{\text{dip}} \propto Ro^{-1.32}$.

To reproduce the spin up on the PMS due to the decrease in the stellar moment of inertia, previous studies have found that core-envelope decoupling must be included (Krishnamurthi et al. 1997). We use the core-envelope decoupling model described by Gallet & Bouvier (2015) and adopt coupling timescales of 30 Myr, 20 Myr, and 10 Myr for the 10th, 50th and 90th percentile tracks, respectively, which we find give us good agreement between the rotational evolution model and the observations. Finally, we assume that during the first few million years, the stellar rotation rates do not evolve with time due to ‘disk-locking’, i.e. magnetic interactions with the circumstellar

disk. We assume disk-locking timescales of 10 Myr, 5 Myr, and 2 Myr for the 10th, 50th and 90th percentile tracks, respectively.

To predict L_X along the rotation tracks, we use the relation derived from MS stars by W11,

$$R_X = \begin{cases} CRo^\beta, & \text{if } Ro \geq Ro_{\text{sat}}, \\ R_{X,\text{sat}}, & \text{if } Ro \leq Ro_{\text{sat}}, \end{cases} \quad (1)$$

where $Ro_{\text{sat}} = 0.13$ is the saturation Rossby number, $R_X = L_X/L_{\text{bol}}$, and $R_{X,\text{sat}} = 10^{-3.13}$ is the saturation R_X value. We use $\beta = -2.7$ (W11). We assume that this relation can be used on the PMS if the evolution of L_{bol} and τ_* are treated correctly. Sanz-Forcada et al. (2011) derived a power law to convert L_X (5-100Å) into EUV luminosity, L_{EUV} (100-920Å), of $\log L_{\text{EUV}} = 4.8 + 0.86 \log L_X$, where L_X and L_{EUV} are in erg s^{-1} .

To calculate the evolution of the stellar radius, L_{bol} , the moment of inertia, and τ_* , we use the stellar evolution models of Spada et al. (2013). However, their τ_* values are approximately a factor of two above those of W11 for 1 M_\odot stars; we therefore normalize τ_* at all ages such that the MS value is consistent with Eqn. 1.

3. X-ray Observations

To test our predictions for X-ray distributions at each age, we collect L_X values of single stars from ROSAT, XMM-Newton, and Chandra of open clusters with ages from 30 Myr to 620 Myr. The clusters are NGC 2547 (30 Myr; Jeffries et al. 2006), α Persei (50 Myr; Prosser et al. 1998), NGC 2451 (50 Myr; Hünsch et al. 2003), Blanco I (50 Myr; Pillitteri et al. 2003), Pleiades (100 Myr; Micela et al. 1999; Stauffer et al. 1994), NGC 2516 (110 Myr; Pillitteri et al. 2006; Jeffries et al. 1997), NGC 6475 (300 Myr; Prosser et al. 1995), and Hyades (620 Myr; Stern et al. 1995). For NGC 6475, since no optical catalogue was available, Prosser et al. (1995) did not report upper limits for the non-detected stars and therefore the percentiles for the distribution of L_X should be considered upper limits. For all MS clusters, except Blanco I where masses were given, we derive masses by converting from $(B - V)_0$ using a relation derived from the An et al. (2007) stellar evolution models. For the PMS cluster NGC 2547, we calculated masses using the

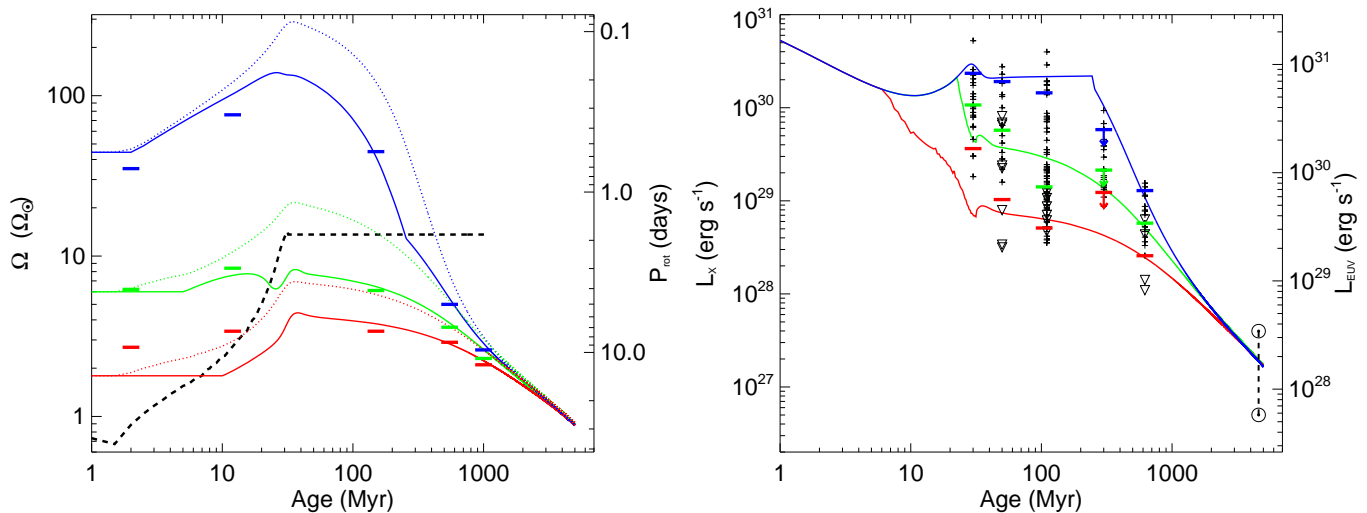


Fig. 2. *Left (a):* Predicted rotational evolution tracks for stars at the 10th (red), 50th (green), and 90th (blue) percentiles of the rotational distribution. The solid and dotted lines show the envelope and core rotational evolution, respectively, and the horizontal solid lines show the observational constraints on the percentiles. The dashed black line shows the time dependent saturation threshold for \dot{M} , B_{dip} , and L_X , calculated assuming a constant saturation R_0 and the τ_* values of Spada et al. (2013). *Right (b):* Predicted L_X along each of our rotation tracks and comparisons to observed L_X values of single stars in several clusters, with upper limits shown by ∇ symbols. The solid horizontal lines show the 10th, 50th, and 90th percentiles of the observed distributions of L_X at each age, calculated by counting upper limits as detections. The two solar symbols at 4.5 Gyr show the range of L_X for the Sun over the course of the solar cycle. The scale on the right y-axis shows the associated L_{EUV} .

Siess et al. (2000) models. Since we use these X-ray observations only to compare to our predictions from rotation, we do not attempt to homogenise the M_* and L_X determinations for each cluster. Our quantitative determinations of the L_X tracks are based on the relation from W11 where such homogenisation was done.

4. Results

Johnstone et al. (2015) combined rotation period measurements of four young clusters with ages of ~ 150 Myr and used a rotational evolution model to predict the evolution of the resulting distribution of Ω on the MS. The sample contains 1556 stars in the $0.4\text{--}1.1 M_\odot$ mass range. In Fig. 1, we show predictions for the distributions of L_X based on these Ω distributions at ages of 150 Myr and 620 Myr comparing with observed values in the Pleiades and Hyades, respectively. There is good overall agreement, although intrinsic X-ray variability (typically factors of 2–3) introduces some additional scatter such as is visible for stars exceeding the saturation threshold.

To predict the range of possible L_X evolution tracks, we calculate rotation models for solar mass stars at the 10th, 50th, and 90th percentiles of the Ω distributions, shown in Fig. 2a. Our models fit well the observational constraints on the percentiles, except for a slight underestimation of the 10th percentile track in the first 20 Myr. This might cause us to underestimate the age when stars on the 10th percentile track come out of saturation by a few Myr. Fig. 2b shows predicted tracks for L_X and L_{EUV} together with observed L_X for stars in the $0.9\text{--}1.1 M_\odot$ range for each cluster listed in Sect. 3. Due to the low number of observations in NGC 2547 (30 Myr), we extend the mass range to $0.8\text{--}1.2 M_\odot$. The tracks correspond very well to the observed percentiles in the individual clusters given the somewhat limited observational samples. The solar L_X ($6 \times 10^{26} - 5 \times 10^{27} \text{ erg s}^{-1}$, Ayres (1997); Peres et al. (2000); Judge et al. (2003);) has been included as well and fits our models excellently.

Stars on our rotation tracks drop out of saturation at ≈ 6 Myr (10th percentile, red), ≈ 20 Myr (50th, green), and ≈ 300 Myr

(90th, blue), i.e., either as young PMS stars, as near-ZAMS stars, or as slightly evolved MS stars. The spread in L_X amounts to as much as 1.5 orders of magnitude for several 100 Myr.

Fig. 3 gives the age when a star falls out of saturation, t_{sat} , as a function of initial Ω , derived from our rotation model. This “saturation time” can be approximated by

$$t_{\text{sat}} = 2.9\Omega_0^{1.14}, \quad (2)$$

where t_{sat} is in Myr and Ω_0 is the rotation rate at 1 Myr in units of the solar rotation rate. Assuming that the saturation level, $L_{X,\text{sat}} \approx 10^{-3.13} L_{\text{bol},\odot}$, is constant in time, which is approximately true, we obtain $\log L_{X,\text{sat}} = 30.46$. If we approximate L_X by a power law after t_{sat} (see Fig. 2b), we obtain, for a given Ω_0 ,

$$L_X = \begin{cases} L_{X,\text{sat}}, & \text{if } t \leq t_{\text{sat}}, \\ at^b, & \text{if } t \geq t_{\text{sat}}. \end{cases} \quad (3)$$

We require that the power law also fits the Sun with $L_{X,\odot} = 10^{27.2} \text{ erg s}^{-1}$ at an age of $t_\odot = 4570$ Myr. We thus find

$$b^{-1} = 0.35 \log \Omega_0 - 0.98, \quad a = L_{X,\odot} t_\odot^{-b}. \quad (4)$$

For the 10th, 50th, and 90th percentiles in Ω_0 , corresponding to $\Omega_0 \approx 1.8\Omega_\odot, 6.2\Omega_\odot$, and $45.6\Omega_\odot$ with $t_{\text{sat}} \approx 5.7$ Myr, 23 Myr, and 226 Myr, respectively, we find

$$L_X = \begin{cases} 2.0 \times 10^{31} t^{-1.12} \\ 2.6 \times 10^{32} t^{-1.42} \\ 2.3 \times 10^{36} t^{-2.50} \end{cases} \quad L_{\text{EUV}} = \begin{cases} 7.4 \times 10^{31} t^{-0.96} \\ 4.8 \times 10^{32} t^{-1.22} \\ 1.2 \times 10^{36} t^{-2.15} \end{cases} \quad \begin{matrix} 10\text{th} \\ 50\text{th} \\ 90\text{th} \end{matrix}$$

where luminosities are in erg s^{-1} . The slope of the median L_X track, $b = -1.42$, is very close to values reported from linear regression to the Sun in Time sample (Güdel et al. 1997; Ribas et al. 2005). These power-law fits, valid for $t > t_{\text{sat}}$, thus describe the range of possible evolutionary tracks for L_X and L_{EUV} .

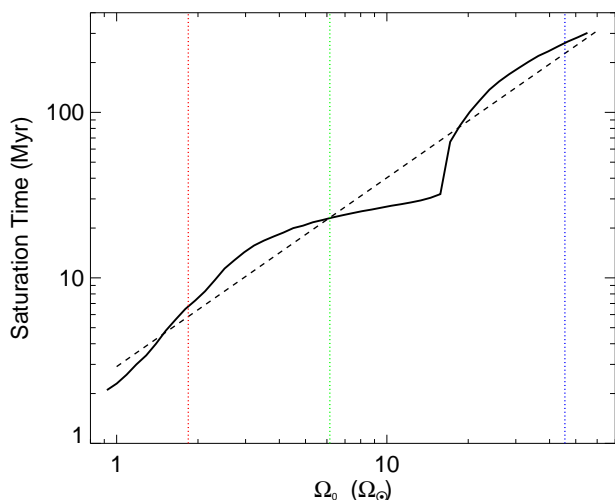


Fig. 3. Saturation time as a function of initial rotation rate Ω_0 . To calculate each rotation track, we fit power laws to the core-envelope coupling timescale and disk-locking timescales for our 10th, 50th, and 90th percentile models of $\tau_{\text{CE}} = 38\Omega_0^{-0.34}$ and $t_{\text{disk}} = 13.5\Omega_0^{-0.5}$, where the timescales are given in Myr and Ω_0 is in solar units. The dashed line shows our best fit, given by Eqn. 2, and the vertical lines show the saturation times of the 10th, 50th, and 90th percentile rotators.

5. Discussion

The large differences in the evolutionary tracks, and therefore L_X and L_{EUV} values, make it necessary to reconsider critically the atmospheric erosion of planets by high-energy radiation. To first approximation, the thermal mass loss rate from a simple hydrogen dominated planetary atmosphere, \dot{M}_{pl} , can be estimated using the energy limited approach (Watson et al. 1981; Lammer et al. 2009), where \dot{M}_{pl} is proportional to the incident stellar EUV flux for a given set of planetary parameters. We therefore assume that $\dot{M}_{\text{pl}} \propto F_{\text{EUV}}$, where F_{EUV} is the EUV flux at the planetary orbit. As an example, we consider the case of a $0.5 M_{\text{Earth}}$ planet at 1 AU around a $1 M_{\odot}$ star with an initial hydrogen atmosphere of $5 \times 10^{-3} M_{\text{Earth}}$. For this case, Lammer et al. (2014) calculated \dot{M}_{pl} from the atmosphere of $3.5 \times 10^{32} m_{\text{H}} \text{ s}^{-1}$ with $F_{\text{EUV}} = 100 \text{ erg s}^{-1} \text{ cm}^{-2}$, where m_{H} is the mass of a hydrogen atom (see the fifth case in their Table 4). We therefore assume that $\dot{M}_{\text{pl}} = 5.9 \times 10^6 F_{\text{EUV}}$, where F_{EUV} is in $\text{erg s}^{-1} \text{ cm}^{-2}$ and \dot{M} is in g s^{-1} .

We show in Fig. 4 the evolution of the planetary atmospheric mass between 10 Myr and 5 Gyr assuming that the central star follows the L_{EUV} tracks shown in Fig. 2. Although in all three cases, the planet at 10 Myr has identical atmospheric masses, by 5 Gyr the atmospheric hydrogen contents are very different. Orbiting the slowly rotating star, the planet retains 45% of its initial atmosphere; orbiting the rapidly rotating star, the planet loses its entire atmosphere within 100 Myr; orbiting the 50th percentile rotator, the planet also loses its atmosphere, but this instead takes almost a Gyr. Although this is a simple calculation of a single example atmosphere, it is sufficient to show that the star's initial rotation rate, and the subsequent rotational evolution, is an important aspect that needs to be properly considered when studying the evolution of terrestrial planetary atmospheres.

Acknowledgements. The authors thank the referee, Nicholas Wright, for valuable comments. LT was supported by an “Emerging Fields” grant of the University of Vienna through the Faculty of Earth Sciences, Geography and Astronomy. CPJ, MG, and HL acknowledge the support of the FWF NFN project

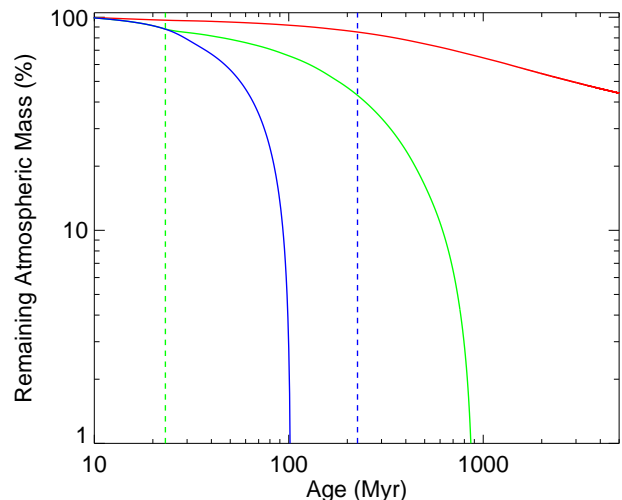


Fig. 4. The evolution of the planetary atmospheric mass of a $0.5 M_{\text{Earth}}$ planet orbiting a $1 M_{\odot}$ star at 1 AU with an initial mass of $5 \times 10^{-3} M_{\text{Earth}}$. The tracks correspond to planets orbiting stars that are on the 10th (red), 50th (green), and 90th (blue) percentiles of the rotational distributions. The vertical lines show the stellar saturation times.

S11601-N16 “Pathways to Habitability: From Disks to Active Stars, Planets and Life”, and the related FWF NFN subprojects S11604-N16 “Radiation & Wind Evolution from T Tauri Phase to ZAMS and Beyond” and S11607-N16 “Particle/Radiative Interactions with Upper Atmospheres of Planetary Bodies Under Extreme Stellar Conditions”. This publication is supported by the Austrian Science Fund (FWF).

References

- An, D., Terndrup, D. M., & Pinsonneault, M. H. 2007, *ApJ*, 671, 1640
 Ayres, T. R. 1997, *J. Geophys. Res.*, 102, 1641
 Gallet, F. & Bouvier, J. 2013, *A&A*, 556, A36
 Gallet, F. & Bouvier, J. 2015, *ArXiv e-prints*
 Güdel, M., Guinan, E. F., & Skinner, S. L. 1997, *ApJ*, 483, 947
 Henderson, C. B. & Stassun, K. G. 2012, *ApJ*, 747, 51
 Hünsch, M., Weidner, C., & Schmitt, J. H. M. M. 2003, *A&A*, 402, 571
 Jeffries, R. D., Evans, P. A., Pye, J. P., & Briggs, K. R. 2006, *MNRAS*, 367, 781
 Jeffries, R. D., Thurston, M. R., & Pye, J. P. 1997, *MNRAS*, 287, 350
 Johnstone, C. P., Güdel, M., Brott, I., & Lüftinger, T. 2015, *ArXiv e-prints*
 Judge, P. G., Solomon, S. C., & Ayres, T. R. 2003, *ApJ*, 593, 534
 Kislyakova, K., Lammer, H., Holmström, M., et al. 2013, *Astrobiology*, 13, 1030
 Kislyakova, K. G., Johnstone, C. P., Odert, P., et al. 2014, *A&A*, 562, A116
 Krishnamurthi, A., Pinsonneault, M. H., Barnes, S., & Sofia, S. 1997, *ApJ*, 480, 303
 Lammer, H., Odert, P., Leitinger, M., et al. 2009, *A&A*, 506, 399
 Lammer, H., Stökl, A., Erkaev, N. V., et al. 2014, *MNRAS*, 439, 3225
 Lichtenegger, H., Lammer, H., Grieblmeier, J., et al. 2010, *Icarus*, 210, 1
 Matt, S. P., MacGregor, K. B., Pinsonneault, M. H., & Greene, T. P. 2012, *ApJ*, 754, L26
 Micela, G., Sciortino, S., Harnden, Jr., F. R., et al. 1999, *A&A*, 341, 751
 Moraux, E., Artemenko, S., Bouvier, J., et al. 2013, *A&A*, 560, A13
 Penz, T., Micela, G., & Lammer, H. 2008, *A&A*, 477, 309
 Peres, G., Orlando, S., Reale, F., Rosner, R., & Hudson, H. 2000, *ApJ*, 528, 537
 Pillitteri, I., Micela, G., Damiani, F., & Sciortino, S. 2006, *A&A*, 450, 993
 Pillitteri, I., Micela, G., Sciortino, S., & Favata, F. 2003, *A&A*, 399, 919
 Prosser, C. F., Stauffer, J. R., Caillault, J.-P., et al. 1995, *AJ*, 110, 1229
 Prosser, C. P., Randich, S., & Simon, T. 1998, *AN*, 319, 215
 Ribas, I., Guinan, E. F., Güdel, M., & Audard, M. 2005, *ApJ*, 622, 680
 Sanz-Forcada, J., Micela, G., Ribas, I., et al. 2011, *A&A*, 532, A6
 Siess, L., Dufour, E., & Forestini, M. 2000, *A&A*, 358, 593
 Skumanich, A. 1972, *ApJ*, 171, 565
 Soderblom, D., Stauffer, J., MacGregor, K., & Jones, B. 1993, *ApJ*, 409, 624
 Spada, F., Demarque, P., Kim, Y.-C., & Sills, A. 2013, *ApJ*, 776, 87
 Stauffer, J. R., Caillault, J.-P., Gagne, M., Prosser, C. F., & Hartmann, L. W. 1994, *ApJS*, 91, 625
 Stern, R. A., Schmitt, J. H. M. M., & Kahabka, P. T. 1995, *ApJ*, 448, 683
 Vidotto, A. A., Gregory, S. G., Jardine, M., et al. 2014, *MNRAS*, 441, 2361
 Watson, A. J., Donahue, T. M., & Walker, J. C. G. 1981, *Icarus*, 48, 150
 Wright, N., Drake, J., Mamajek, E., & Henry, G. 2011, *ApJ*, 743, 48 (W11)